JOURNAL OF GEOPHYSICAL RESEARCH, VOL. 105, NO. C11, PAGES 26,301–26,312, NOVEMBER 15, 2000

Bio-optical properties and remote sensing ocean color algorithms for Antarctic Peninsula waters

H. M. Dierssen and R. C. Smith

Institute for Computational Earth System Science, Department of Geography
University of California, Santa Barbara

Abstract. Increasing evidence suggests that bio-optical properties of Antarctic waters are significantly different than those at temperate latitudes. Consequently, retrieval of chlorophyll concentrations from remotely sensed reflectance measurements using standard ocean color algorithms are likely to be inaccurate when applied to the Southern Ocean. Here we utilize a large bio-optical data set (>1000 stations) collected in waters west of the Antarctic Peninsula in conjunction with the Palmer Long Term Ecological Research program to assess ocean optical properties and associated ocean color algorithms. We find that the remote sensing reflectance spectrum as a function of chlorophyll concentrations appears significantly different from the Sea-viewing Wide Field-of-view Sensor (SeaWiFS) Bio-optical Algorithm Mini-workshop data set collected from other regions of the world's oceans. For Antarctic waters, remote sensing reflectance is significantly higher in the blue region and lower in the green region of the spectrum for high chlorophyll concentrations (>1 mg Chl m^{-3}). Therefore applying general processing algorithms for both Coastal Zone Color Scanner and SeaWiFS in these Antarctic waters results in an underestimate of chlorophyll by roughly a factor of 2. From modeled estimates of absorption and backscattering we hypothesize that both low chlorophyll-specific absorption and low backscattering contribute to the high reflectance ratios.

1. Introduction

In assessing the oceanic role in possible climate change, the processes that control the temporal fluxes of carbon into the ocean are important to understand and quantify. The major carbon flux in the ocean is carbon dioxide uptake by phytoplankton during photosynthesis, which can be directly related to the amount of phytoplankton biomass. For Antarctic coastal waters, *Dierssen et al*. [2000] have shown that primary production is tightly coupled to chlorophyll concentrations and can be accurately modeled. However, large-scale shipboard estimates of chlorophyll concentrations for the Southern Ocean are relatively limited. The use of remotely sensed observations from satellites is therefore essential in order to gain a synoptic understanding of the abundance and distribution of phytoplankton. This paper is directed at understanding the bio-optical properties of the Antarctic Peninsula waters and determining optimum algorithms for retrieving chlorophyll concentrations from remotely sensed ocean color observations in these waters.

Recent studies present evidence that bio-optical properties, and hence the relationship between water-leaving radiance and pigment concentrations, are significantly different in the Southern Ocean compared to other oceanic regions [*Mitchell and Holm-Hansen*, 1991; *Mitchell*, 1992; *Sullivan et al*., 1993; *Fenton et al*., 1994; *Arrigo et al*., 1998]. The general processing algorithm for retrieving pigment biomass concentrations from the Coastal Zone Color Scanner (CZCS) was found to underestimate low chlorophyll concentrations (<1.5 mg Chl m^{-3}) in the Southern Ocean by a factor of 2.4 [*Mitchell and Holm-Hansen*, 1991; *Sullivan et al*., 1993]. Therefore a regional algorithm was developed for the Southern Ocean [*Sullivan et al*., 1993]. The underestimation by the general algorithm was hypothesized to be due to the low concentrations of detritus and the large pigment-packaging effects in this region, which alter the absorption coefficients in Antarctic waters [*Mitchell and Holm-Hansen*, 1991]. Both pigment-packaging effects and low concentrations of colored dissolved and detrital material would result in a reduced absorption coefficient, an increase in remote sensing reflectance, and an underestimation of chlorophyll concentrations. However, pigment-specific absorption in Southern Ocean waters may vary depending on the species composition of the water column [*Brody et al*., 1992; *Arrigo et al*., 1998].

While absorption properties may be different for Antarctic waters, backscattering coefficients may also play a role in defining the unique relationship between water-leaving radiance and pigment concentrations. Indeed, recent measurements of backscattering in the Antarctic have found low levels of backscattering [*Stramski et al*., 1998; *Dierssen and Smith*, 2000]. Modeling results suggest that particles <0.1 μm are responsible for the majority of backscattering in the oceans [*Morel*, 1991; *Stramski and Kiefer*, 1991]. While submicron microbes and viruses contribute to the total backscattering, the majority of backscattering is thought to come from submicron detrital particles ("Koike" particles <0.06 μm) that have high water content and corresponding low refractive index [*Stramski and Kiefer*, 1991; *Balch et al*., 1998]. Although little is known about the concentrations of Koike particles in the Antarctic, the concentrations of submicron bacterial populations have been found to be low. Compared to most oceanic regions where bacterial biomass is ≥10% of the contemporaneous phytoplankton standing stock, bacterial biomass in the Antarctic Peninsula region is found to be <1–2% of phytoplankton standing stock and generally uncoupled from phytoplankton

Paper number 1999JC000296.
0148-0227/00/1999JC000296$09.00

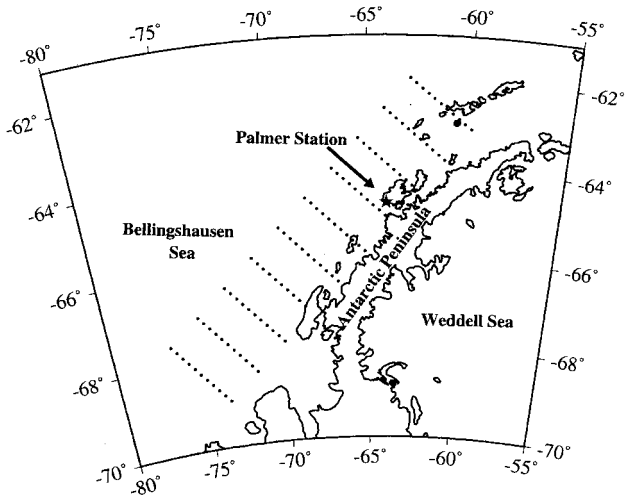

Figure 1. Location of the large-scale LTER sampling grid in reference to Palmer Station, Antarctica.

populations [*Karl et al*., 1996]. Moreover, low bacterial biomass has been found for nearly all Southern Ocean marine ecosystems studied [*Lancelot et al*., 1989; *Cota et al*., 1990; *Zdanowski and Donachie*, 1993]. Given low populations of the submicron bacterial populations and the possibility that microbial decomposition may contribute to the formation of Koike particles [*Stramski and Kiefer*, 1991], the concentrations of backscattering Koike particles might also be similarly low. If particulate backscattering is generally lower in Antarctic waters, then the water-leaving radiance and remote sensing reflectance ($R_{rs}(\lambda)$) would also be lower, and remote sensing pigment retrieval algorithms for the Southern Ocean would also be different when compared to low latitudes.

In this study we use a multiyear data set collected in waters west of the Antarctic Peninsula from 1991–1997 to investigate the bio-optical properties for this region. Optical measurements have been collected with several instruments including the Bio-Optical Profiling System (BOPS-II) [*Smith et al*., 1997], the Optical Free-Fall Instrument (OFFI) [*Waters et al*., 1990], and a Bio Spherical Instruments Profiling Reflectance Radiometer (PRR) operated in a free-fall configuration. The data have been collected over different seasons and years and in waters with both low and high pigment biomass concentrations. Optical observations in this region are especially challenging because of low Sun angles, a corresponding long atmospheric path length, frequent cloudiness (typically 95%), and the presence of sea ice and snow. In section 2 we describe in detail the various data quality issues involved in compiling and processing this Antarctic bio-optical data set. This data set is unique because of the varied spatial and temporal coverage, the careful calibration history for each optical sensor, and the intercomparison of data from different ships, instrumentation, and sampling methodology. These long-term ecological research (LTER) data are compared to a large global data set compiled primarily from temperate waters Sea-viewing Wide Field-of-view (SeaWiFS) Bio-optical Algorithm Mini-workshop (SeaBAM) [*O'Reilly et al*., 1998] and to the CZCS and Sea-viewing Wide Field-of-view Sensor (SeaWiFS) pigment retrieval algorithms.

2. Methods

2.1. Data Collection

Bio-optical data were collected west of the Antarctic Peninsula and from near Palmer Station (64°S, 64°W, Figure 1) from November 1991 to March 1998. Data were obtained using two basic modes of sampling: (1) weekly time series data collected roughly between November and March over a fine-scale grid near Palmer Station and (2) regional data collected during 6 week research cruises that covered a large-scale fixed sampling grid [*Waters and Smith*, 1992]. Table 1 lists the various cruises and optical instrumentation from which data were obtained for this paper. For the seasonal time series data from 1991 to 1994 an Optical Free-Fall Instrument (OFFI) was used to mitigate potential perturbation effects of the ship [*Waters et al*., 1990]. This instrument was replaced by a free-falling Profiling Reflectance Radiometer (PRR), which was used for the nearshore time series data from 1994 onward and for the January 1998 cruise. The BOPS-II instrument [*Smith et al*., 1997] was used to collect optical data for all of the research cruises prior to January 1998. Coincident chlorophyll and conductivity-temperature-depth (CTD) data were also collected with the optical data. Chlorophyll *a* concentrations were estimated by subtracting the phaeopigment concentration determined by sample acidification [*Smith et al*., 1981].

2.2. Optical Calibration

Wherever possible, we used long-term average calibration values to process the bio-optical data. With the exception of a few wavelength channels that degraded over time (and were subsequently replaced) the calibrations generally varied by less than a few percent over the many years of sampling [*Smith et al*., 1997]. Following standard radiometric procedures, instrument calibrations were performed periodically (typically before and after each field deployment) and were carried out at the Ocean Optics Calibration Facility, University of California, Santa Barbara, which participates in the SeaWiFS optical calibration laboratory round robin exercises [*Mueller and Austin*, 1995]. Immersion coefficients were measured for each instrument individually and applied to the calibration of downwelling (E_d) and upwelling (E_u) irradiance data. The measured immersion coefficients for the BOPS-II resulted in irradiances that were 2–6% lower than those measured using the manufacturer-supplied immersion coefficients. Immersion coefficients on upwelling radiance, L_u, were theoretically computed from different refraction indices for water and the clear acrylic window.

2.3. Depth Offsets

The zero depth offset was individually determined for each instrument and each cast. Once the zero depth offset was determined for each cast, we corrected for the positioning of each of the sensors on the instrumentation. For each of the instruments and their respective configurations, we applied an offset to the measured depths to account for the distances between the downwelling and upwelling sensors on the instrumentation package. Thus the data matrices from each sensor were realigned such that the depth corresponded to the true depth of each individual sensor in the water column and not the depth of the pressure sensor. Table 1 shows the size of each instrument and the distance between the downwelling and upwelling sensors for each of the three instruments.

Table 1. Optical Instrumentation Used for LTER Sampling

	Optical Instrument	Size,[a] m Diameter × Length	Instrument Identification Numbers	Wavelengths[b]			
				E_d	E_u	L_u	E_s
cruise							
nov91	BOPS-II	0.83 × 1[c]	8714[d]/8715[e]/8709	1	1	1	2
jan93	BOPS-II	0.83 × 1[c]	8714[d]/8715[e]/8709	1	1	1	2
aug93	BOPS-II	0.83 × 1[c]	8714[d]/8715[e]/8709	1	1	1	2
jan94	BOPS-II	0.83 × 1[c]	8714[d]/8715[e]/8709	1	1	1	2
jan95	BOPS-II	0.83 × 1[c]	8714[f]/8715[e]/8722	3	1	1	7
jan96	BOPS-II	0.83 × 1.3[g]	8714[f]/8715[h]/8709	3	1	1	2
jan97	BOPS-II	0.83 × 1.3[g]	8714[f]/8715[h]/8709	3	1	1	2
jan98a/b	PRR	0.2 × 0.40	9628[i]/9629	4	···	4	4
jan99	PRR	0.2 × 0.40	9603/9614	6	···	6	6
station							
pal9192	OFFI	0.2 × 0.75	8722/8709	5	···	5	2
pal9293	OFFI	0.2 × 0.75	8722/8709	5	···	5	2
pal9394	OFFI	0.2 × 0.75	8722/8709	5	···	5	2
pal9495	PRR	0.2 × 0.40	9603/9614	6	···	6	6
pal9596	PRR	0.2 × 0.40	9628/9629	4	···	4	4
pal9697	PRR	0.2 × 0.40	9628/9629	4	···	4	4
pal9798	PRR	0.2 × 0.40	9628[i]/9629	4	···	4	4

[a]Except where specified, the length is the distance between the E_d and L_u/E_u sensors, and the sensors are centered on the instrumentation array.
[b]Wavelength (nm) are 1: 410, 441, 488, 520, 565, and 625; 2: 410, 441, 488, and 560; 3: 410, 412, 441, 443, 488, 490, 510, 520, 555, 565, 589, 625, and 665; 4: 412, 443, 490, 510, 555, and 665; 5: 410, 441, 488, 520, 565, and 765; 6: 412, 443, 490, 510, 555, and 656; and 7: 38 channels.
[c]L_u sensor 10 cm above bottom of array and mounted on one side of instrument.
[d]Pre-November 1994 long-term average, 8 channels.
[e]Pre-October 1995 long-term average.
[f]Post-November 1994 long-term average, 13 channels.
[g]L_u sensor 40 cm above bottom of array and mounted on one side instrument.
[h]Post-October 1995 long-term average, decreased the acceptance angle on sensor.
[i]New teflon diffuser put on 9628.

2.4. Extrapolation to the Surface

For typical sea states it is not practical to make optical measurements precisely at an infinitesimal depth below (or above) the surface. Consequently, profiles of irradiance ($E_d(z, \lambda)$) and radiance ($L_u(z, \lambda)$) were measured in the upper few optical depths, and estimates just beneath the sea surface ($z = 0^-$) were obtained by propagating the measurements back to the sea surface using a least squares regression technique to estimate the downwelling and upwelling attenuation coefficients, $K_d(\lambda)$ or $K_L(\lambda)$ [*Smith and Baker*, 1984], such that

$$\ln [E_d(0^-, \lambda)] = \ln [E_d(z, \lambda)] + K_d(\lambda) z, \quad (1)$$

$$\ln [L_u(0^-, \lambda)] = \ln [L_u(z, \lambda)] + K_L(\lambda) z, \quad (2)$$

$$R_{rs}(0^-, \lambda) = \frac{L_u(0^-, \lambda)}{E_d(0^-, \lambda)}. \quad (3)$$

Measured radiation from different depth intervals of 0.5–5 m were used in the regression to obtain estimates of $L_u(0^-, \lambda)$ and $E_d(0^-, \lambda)$. As confirmation of our extrapolation process, we found a strong coherence between $R_{rs}(0^+, \lambda)$ estimated from $E_d(0^-, \lambda)$ and $R_{rs}(0^+, \lambda)$ estimated from measured downwelling irradiance above the sea surface, $E_d(0^+, \lambda)$ (as measured from a shipboard sensor). Spectral remote sensing reflectance just below the air-water interface, $R_{rs}(0^-, \lambda)$, was then estimated as the ratio of $L_u(0^-, \lambda)$ to $E_d(0^-, \lambda)$ (equation (3)).

2.5. Remote Sensing Reflectance $R_{rs}(0^+, \lambda)$

For much of the following analyses we use remote sensing reflectance estimated just above the sea surface, $R_{rs}(0^+, \lambda)$. We estimate $R_{rs}(0^+, \lambda)$ using the reflectance measured just beneath the surface $R_{rs}(0^-, \lambda)$ (equation (3)) in the following relationship [*Smith and Baker*, 1986; *Mobley*, 1994; *Mueller*, 1995]:

$$R_{rs}(0^+, \lambda) = t_r(\lambda) R_{rs}(0^-, \lambda) \quad (4)$$

$$t_r(\lambda) = \frac{1 - \rho(\lambda, \theta)}{n_w^2(\lambda)} t_d. \quad (5)$$

Here we assume that the Fresnel reflectance from water to air, $\rho(\lambda, \theta)$, is 0.021–0.022. Depending on the wavelength, we use the wavelength-specific index of refraction, n_w, for water at 0°C [*Austin and Halikas*, 1976; *Mobley*, 1994] and assume that the transmittance of $E_d(0^+)$ across the sea surface, t_d, is 0.96 [*Smith and Baker*, 1986; *Dierssen and Smith*, 1997]. The resultant transmittance factor t_r used to convert $R_{rs}(0^-, \lambda)$ to $R_{rs}(0^+, \lambda)$ varied from 0.515 to 0.524 depending on wavelength. This is consistent with the methodology used to process the SeaBAM data set [*O'Reilly et al.*, 1998] and with modeling results from Hydrolight [*Mobley*, 1994], which show that 51–54% of the $R_{rs}(0^-, \lambda)$ signal is propagated through the sea surface depending on the wavelength, absorption, scattering, and wind and sky conditions.

2.6. Instrument Self-Shading

In order to avoid significant instrument self shading the instrument radius r must be less than $(30a(\lambda))^{-1}$ for $E_u(\lambda)$ and $(100a(\lambda))^{-1}$ for $L_u(\lambda)$ [*Gordon and Ding*, 1992], where a is the absorption coefficient for the water column. In these waters, chlorophyll concentrations over 30 mg Chl m^{-3} are known to occur and estimates of absorption can be over 0.4 m^{-1} (see section 4.2). Consequently, under high chlorophyll

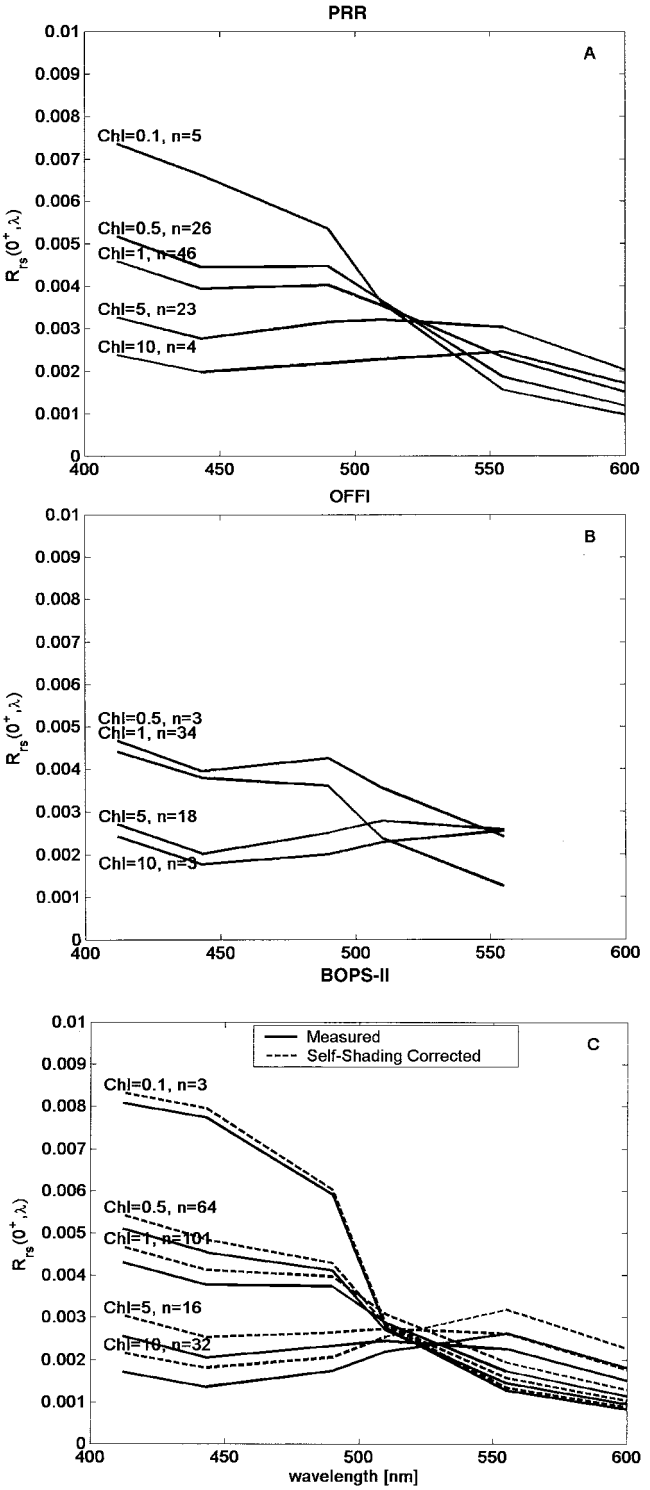

Figure 2. Median spectral measurements of $R_{rs}(0^+, \lambda)$ for various concentrations of chlorophyll (±20%) using data from (a) PRR, (b) OFFI, and (c) BOPS-II measured and self-shading corrected.

situations the radius of our instruments would need to be <2.5 cm to obtain accurate upwelling radiance measurements. Since the BOPS-II instrument is mounted on a large diameter rosette (radius 42 cm; Table 1), we investigated techniques for correcting instrument self-shading effects on the upwelling radiance and irradiance data. Self-shading correction techniques have been derived and tested primarily for low chlorophyll situations in which the product of a and r is <0.1 [*Gordon and Ding*, 1992; *Mueller and Austin*, 1995; *Zibordi and Ferraro*, 1995]. Because we did not have coincident absorption measurements for these data, we followed an approach recently tested in more productive coastal waters [*Aas and Korsbo*, 1997], which used the upwelling diffuse attenuation coefficients K_L combined with the instrument radius r and a scaling factor B, such that

$$\ln [L_u^{\text{meas}}(\lambda)] = \ln [L_u^{\text{true}}(z, \lambda)] - BK_L(\lambda)r \qquad (6)$$

Aas and Korsbo [1997] found that this approach was applicable to highly absorbing waters and yielded error estimates that were within 7% of those estimated from the model of *Gordon and Ding* [1992]. From their measurements the scaling factor B was found to be dependent both on wavelength and Sun angle and ranged between 1.6 and 2.5. To process the BOPS-II data, we used B coefficients of 2.0, 2.3, 1.8, 1.6, 2.2, and 2.5 corresponding to a Sun angle of 50° and the wavelengths 410, 441, 488, 520, 565, and 625 nm, respectively. The BOPS-II E_u data were processed using the above B coefficients scaled by 0.586 (i.e., $k_{\text{sky}}(E_u)/k_{\text{sky}}(L_u)$ from *Zibordi and Ferraro* [1995]). Determining the appropriate radius was problematic for the BOPS-II instrument because the upwelling radiance sensor was mounted on one side of the instrument, and hence it was not shaded symmetrically by the instrument. To be conservative, we assumed that the instrument was shaded equally by the full instrument radius (0.42 m).

The self-shading corrections varied from a few percent for the low chlorophyll concentrations to around 40% for the higher chlorophyll concentrations. Because of the numerous uncertainties inherent in these self-shading corrections, the corrected BOPS-II data were carefully compared to the PRR and OFFI data, which are smaller instruments that do not have significant self-shading problems. In Figure 2, we compare median $R_{rs}(0^+, \lambda)$ estimated for the free-falling PRR (Figure 2a), OFFI (Figure 2b), and the BOPS-II instrument (Figure 2c) for different chlorophyll concentrations (±20%). Overall, the corrected $R_{rs}(0^+, \lambda)$ for the BOPS-II match up closely in magnitude and overall shape to the PRR and OFFI data. When used concurrently, the corrected BOPS-II estimates were found to be within the experimental error of data obtained using the OFFI or PRR instruments and are used throughout the remainder of this paper.

2.7. Wavelength Differences

The spectral bands for discrete wavelength filters on the BOPS-II and OFFI radiometers (410, 441, 488, 520, 565, and 625/765 nm) are different from the recommended SeaWiFS spectral bands incorporated in the PRR (412, 443, 490, 510, 555, and 665 nm). The first three wavelengths for these instruments are within 2 nm of each other and are used interchangeably throughout this paper. The last three wavelengths have larger differences between the three instruments (>10 nm). Since the spectral shape of remote sensing reflectance is unique for these data as compared to temperate data, wavelength corrections determined for low chlorophyll temperate waters [*O'Reilly et al.*, 1998] may not be appropriate for these waters. Therefore, rather than applying wavelength corrections, we present the data separately for each instrument and wavelength ratio so as to ensure that no bias is presented by using mixed wavelength ratios.

2.8. Data Quality Assurance

The presence of inorganic particles in the water column (e.g., from glacial runoff) can cause the water's optical properties to be uncoupled from chlorophyll concentrations. Under these conditions the waters are considered to be case 2 and should be treated separately from case 1 waters [*Gordon and Morel*, 1983]. While specific delineations have not been established to distinguish between case 1 and case 2 waters for the Southern Ocean, we generally find a tight coupling between the reflectance ratios and chlorophyll concentrations, which is indicative of case 1 waters. Approximately 165 of our 1248 stations were deemed to have anomalously high reflectance and a flatter spectral shape that was consistent with case 2 waters. These case 2 data were predominantly associated with glacial melt conditions (i.e., low-salinity surface lens) and are excluded from this analysis of case 1 data. A discussion of case 2 waters will be presented elsewhere. Without these case 2 data the final data set used in the remainder of this paper consisted of 1083 stations.

3. Results

In order to understand how the bio-optical properties of Antarctic waters differ from other oceanic regions we have compared the Antarctic LTER data to the global SeaBAM data [*O'Reilly et al.*, 1998]. The SeaBAM data set ($n = 919$) is a compilation of coincident chlorophyll and remote sensing reflectance measurements primarily from nonpolar mesotrophic case I waters. Both data sets have lognormally distributed chlorophyll concentrations and cover a wide range of pigment biomass concentrations. The SeaBAM data set has more stations in the lower range of chlorophyll concentrations (median of 0.2 mg Chl m^{-3}) and ranges from 0.02 to 33 mg Chl m^{-3}. In contrast, the median chlorophyll concentration for these LTER data is higher at around 1 mg Chl m^{-3} and ranges from 0.7 to 43 mg Chl m^{-3} (Figure 3). In comparison to the SeaBAM data the LTER data have considerably more high chlorophyll stations (>5 mg Chl m^{-3}) and virtually no oligotrophic data (<0.1 mg Chl m^{-3}). However, both data sets are large and overlap in their ranges.

Figure 4 shows measurements of chlorophyll versus $R_{rs}(0^+, 443)$ for the SeaBAM data (Figure 4a) and the LTER data from the BOPS-II (Figures 4b and 4c), OFFI (Figure 4d), and PRR (Figure 4e) instruments, respectively. The data are presented for each instrument and then combined in Figure 4f for ease of illustration and discussion. For data from all three LTER instruments, $R_{rs}(0^+, 443)$ is generally higher than the best polynomial fit to the SeaBAM (shown as the dotted line on all of the subplots). The data collected during the winter cruises in early November 1991 and August 1993 were consistently found to be lower than the SeaBAM data (Figure 4c). This could be due to the low incoming irradiance and very high solar zenith angles associated with winter months in the Antarctic. If we exclude the BOPS-II winter data, the blue reflectance values from the LTER data set are consistently higher than the SeaBAM data set. Above values of about 10 mg Chl m^{-3}, too few SeaBAM data are available to make a reliable comparison.

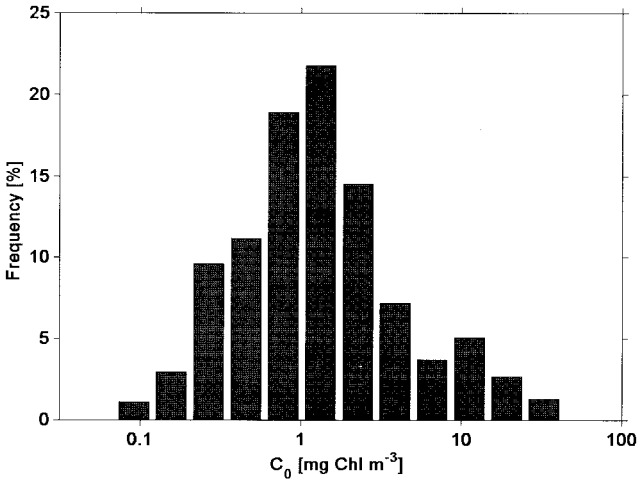

Figure 3. Lognormal frequency distribution of all LTER surface chlorophyll concentrations.

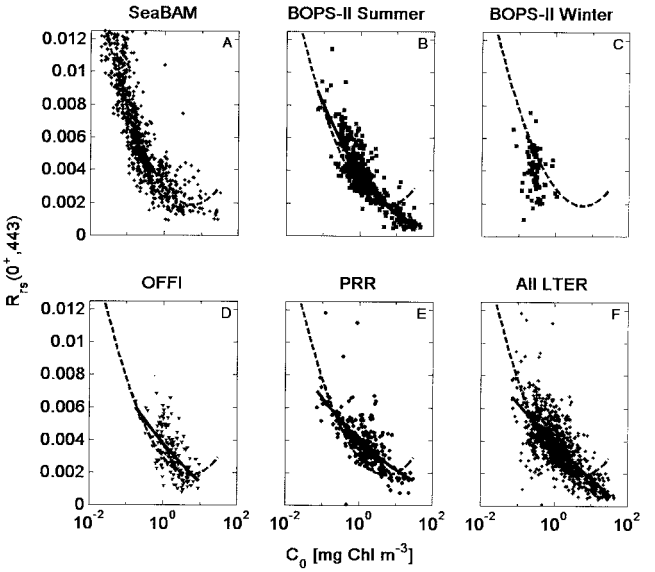

Figure 4. Surface chlorophyll versus $R_{rs}(0^+, 443)$ for (a) SeaBAM, (b) BOPS-II summer (December–March), (c) BOPS-II winter (April–November), (d) OFFI, (e) PRR, and (f) all LTER data. Solid lines are best fits to plotted data, and dotted lines are best fits to SeaBAM data derived in Figure 4a. No best fit was possible for Figure 4c.

The panels in Figure 5 are identical to those in Figure 4 except the data are from the green region of the spectrum, $R_{rs}(0^+, 555–565)$. The reflectance data for the BOPS-II and OFFI are for a waveband centered at 565 nm, whereas the PRR and most of the SeaBAM data are centered at 555 nm. Because significant differences in reflectance can occur between 555 and 565 nm, caution must be taken when concluding from Figure 5 that $R_{rs}(0^+, 555)$ is generally lower for the LTER data than for the SeaBAM data. As shown in Figure 5a, the SeaBAM data set also contains reflectance measured at both 555 and 565 nm. Because the SeaBAM $R_{rs}(0^+, 555)$ are primarily from low chlorophyll stations (<1 mg Chl m^{-3}) and because the reflectance spectra is most steeply sloped at low chlorophyll concentrations, these data were found to be ~20% lower than $R_{rs}(0^+, 555)$ [*Balch et al.*, 1998; *O'Reilly et al.*, 1998]. At higher chlorophyll concentrations, however, the difference between reflectance at these two wavelengths is reduced, and $R_{rs}(0^+, 565)$ can be equal to or even greater than $R_{rs}(0^+, 555)$. From the 555 nm PRR data (Figure 5e) we can

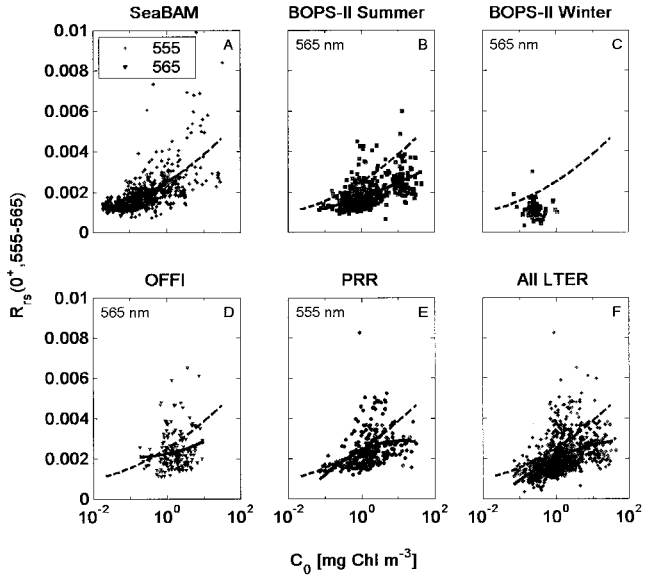

Figure 5. Same as Figure 4 except for a different wavelength, $R_{rs}(0^+, 555)$. BOPS-II and OFFI data (Figures 4b–4d) are $R_{rs}(0^+, 565)$.

conclude that the green reflectance for the LTER data is lower than the corresponding SeaBAM for high chlorophyll concentrations (>5 mg Chl m^{-3}). This difference is statistically significant, as discussed below.

We have also averaged the data to compare wavelength-specific $R_{rs}(0^+, \lambda)$ measured for increasing concentrations of chlorophyll (±20%) for the SeaBAM and LTER data (Figure 6). Consistent with Figures 4 and 5, the LTER and SeaBAM reflectance spectra are significantly different both in the blue and green regions. At high chlorophyll concentrations (>5 mg Chl m^{-3}) the LTER reflectance is lower in the green than the SeaBAM data. In addition, the LTER reflectance in the blue region of the spectrum (410–443 nm) is generally higher than the SeaBAM at chlorophyll concentrations >0.1 mg Chl m^{-3}.

Statistical *t* tests comparing the SeaBAM and the PRR data for each wavelength and chlorophyll category are shown in Table 2. Because of the wavelength differences between the SeaBAM data and the BOPS-II and OFFI data, we have only used the PRR data for this statistical comparison. This is also a conservative statistical test because only 311 of the 1124 stations are from the PRR instrument. For a given wavelength and chlorophyll concentration, Table 2 presents the relative percent difference between the mean value from each data set and the results of the hypothesis test that the means of the two data sets are equal. A value of 0 indicates that we would accept the null hypothesis that the means are equal at a significance level of 0.05. A value of 1 or −1 indicates that the mean of the LTER data is significantly greater or less, respectively, than the SeaBAM data. The PRR reflectance is significantly lower than the SeaBAM data (up to 40% lower) for high chlorophyll concentration and green wavelengths. The PRR reflectance is significantly greater than SeaBAM at chlorophyll concentrations of 0.5 mg Chl m^{-3} across most of the spectrum. The PRR reflectance at 412 nm is also statistically greater at 5 mg Chl m^{-3}. For nearly all chlorophyll levels the LTER reflectance is on average lower than the SeaBAM data for greener wavelengths (>490 nm) and is greater than the SeaBAM data for bluer wavelengths (<490 nm).

The standard satellite pigment retrieval algorithms for both CZCS and SeaWiFS utilize the fact that the ratios of remotely sensed radiance vary in a systematic way with chlorophyll concentration. As seen from the spectral shapes in Figure 6, chlorophyll can be estimated by comparing the reflectance in the blue to that in the green. The ratios of blue to green reflectance should be >1 for low chlorophyll concentrations and <1 at high chlorophyll concentrations. However, because the LTER reflectance spectra is significantly different from the SeaBAM spectra (Table 2), we expect the resulting waveband ratios also to be significantly different. The general processing algorithm for CZCS makes use of the ratio of $L_u(443)/L_u(555)$ for chlorophyll and phaeopigment concentrations <1.5 mg Chl m^{-3} and the ratio $L_u(520)/L_u(555)$ for concentrations >1.5 mg Chl m^{-3}. For concentrations <1.5 mg Chl m^{-3}, Southern Ocean researchers have found that the CZCS general processing algorithm underestimates biomass by a factor of ~2.4 [*Mitchell and Holm-Hansen*, 1991; *Sullivan et al.*, 1993].

Figure 7 compares the performance of the CZCS general processing algorithms for the LTER data. For chlorophyll and phaeopigment <1.5 mg Chl m^{-3} the $L_u(443)/L_u(555)$ algorithm (Figure 7a) tends to underestimate LTER chlorophyll concentrations by roughly a factor of 2. Our data is consistent with the (RACER) data also collected west of the Antarctic Peninsula [*Mitchell and Holm-Hansen*, 1991] and with data collected from cryptophyte-dominated waters in the Ross Sea [*Arrigo et al.*, 1998]. Our best model II regression line [*Laws and Archie*, 1981] ($r^2 = 0.56$) is significantly higher than the

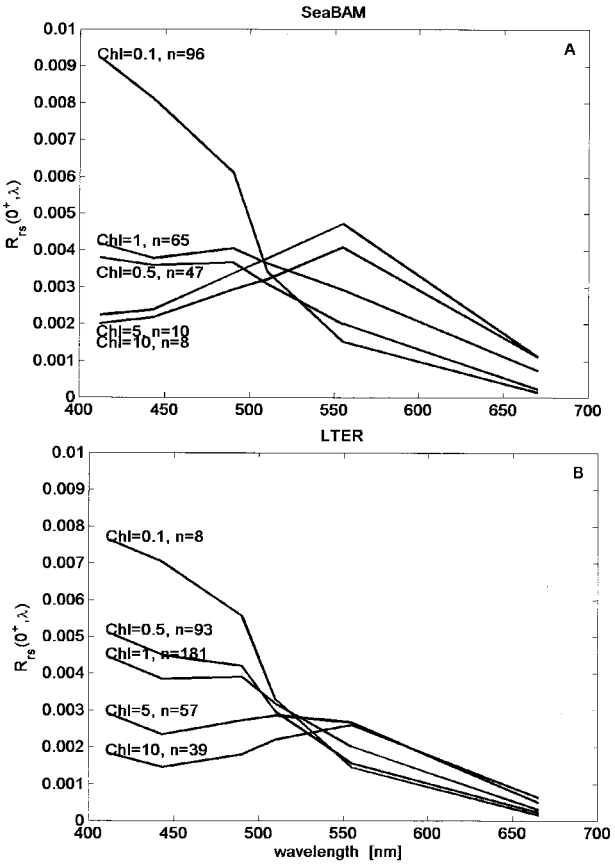

Figure 6. Median spectral measurements of $R_{rs}(0^+, \lambda)$ for various concentrations of chlorophyll (±20%) using data from (a) SeaBAM and (b) LTER.

Table 2. Statistical Results From a *t* Test[a] Comparing Measured SeaBAM and PRR $R_{rs}(0^+, \lambda)$ for Different Chlorophyll Concentrations[b]

Chlorophyll,[b] mg m^{-3}	Wavelength, nm				
	412	443	490	510	555
0.1	0 (−20%)	0 (−19%)	0 (−13%)	0 (5%)	0 (3%)
0.5	1 (36%)	1 (24%)	1 (22%)	1 (18%)	0 (−7%)
1	0 (10%)	0 (4%)	0 (−1%)	0 (−3%)	−1 (−20%)
5	1 (46%)	0 (16%)	0 (−6%)	0 (−15%)	−1 (−36%)
10	0 (18%)	0 (−9%)	0 (−25%)	0 (−29%)	−1 (−40%)

[a]Assuming a significance level of 0.05, the statistical results are as follows: 0, accept the null hypothesis that the means are equal; 1, reject the null hypothesis and accept the alternative hypothesis that the LTER mean is greater than the SeaBAM mean; and −1, reject the null hypothesis and accept the alternative hypothesis that the LTER mean is less than the SeaBAM mean. The number in parenthesis represents the percent difference between mean LTER and SeaBAM values.

[b]Chlorophyll categories are ±20% of the value given.

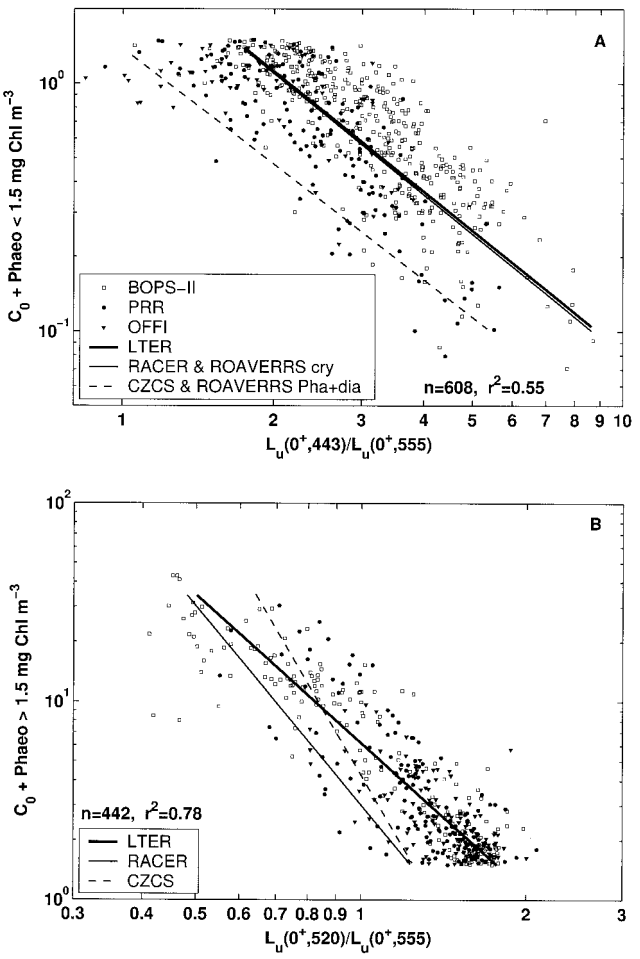

Figure 7. Water-leaving radiance ratios used in the CZCS general processing algorithm: (a) the ratio of $L_u(443)/L_u(555)$ for chlorophyll and phaeopigment concentrations <1.5 mg Chl m^{-3} and (b) the ratio $L_u(520)/L_u(555)$ for chlorophyll concentrations >1.5 mg Chl m^{-3}. The thick solid lines are the best fit lines for all LTER data, and the dashed lines represent the general processing CZCS algorithms [*Gordon and Morel*, 1983]. The RACER data are from Antarctic Peninsula waters [*Mitchell and Holm-Hansen*, 1991]. The Research on Ocean-Atmosphere Variability and Ecosystem Response in the Ross Sea (ROAVERRS) data are from the Ross Sea [*Arrigo et al*., 1998], where cryp is cryptophytes, Pha is *Phaeocystis Antarctica*, and dia is diatoms.

general processing CZCS algorithm [*Gordon and Morel*, 1983] and reflectance data collected from diatom and *Phaeocystis antarctica*-dominated waters in the Ross Sea [*Arrigo et al*., 1998]. For chlorophyll and phaeopigment >1.5 mg Chl m^{-3} the CZCS general processing algorithm using $L_u(520)/L_u(555)$ (Figure 7; dashed line) is also inaccurate for these LTER data. When compared to the LTER regression line ($r^2 = 0.78$), the CZCS algorithm underestimates chlorophyll for concentrations >10 mg Chl m^{-3} and overestimates chlorophyll for concentrations >10 mg Chl m^{-3}. Thus chlorophyll determined from CZCS is underestimated not only at low chlorophyll concentrations, as previously noted [*Sullivan et al*., 1993], but also at concentrations up to ~10 mg Chl m^{-3}.

Table 3 presents the coefficients for the CZCS radiance ratio algorithms derived from these LTER data and also presents the corrections that can be applied to the chlorophyll concentrations once they have already been processed with the CZCS algorithm. The factor of ~2.22 can be linearly applied to the CZCS satellite-derived chlorophyll concentrations <1.5 mg Chl m^{-3}. For Antarctic coastal waters, chlorophyll concentrations derived from the $L_u(520)/L_u(555)$ CZCS algorithm can be corrected using a log linear equation (Table 3) to increase concentrations <10 mg Chl m^{-3} and decrease concentrations >10 mg Chl m^{-3}.

The ocean color algorithm for SeaWiFS (Ocean Color 2 wavelength version 2 (OC2V2)) utilizes a modified cubic polynomial function to derive chlorophyll concentrations from the reflectance ratio $R_{rs}(490)/R_{rs}(555)$ [*O'Reilly et al*., 1998]. By normalizing water-leaving radiance ratios to the downwelling irradiance (i.e., using R_{rs} instead of L_u) the data appear less variable compared to the CZCS algorithms, and the SeaWiFS algorithm explains more of the variability in the data. For nearly the entire range of chlorophyll the LTER $R_{rs}(490)/R_{rs}(555)$ ratios are consistently higher per unit of chlorophyll than those derived with the OC2V2 algorithm (Figure 8). Figure 8a presents the reflectance ratios versus measured chlorophyll concentrations for the LTER data. Figure 8b presents the measured chlorophyll versus the chlorophyll that would be derived using the measured reflectance ratios and the OC2V2 algorithm. As shown, the OC2V2 algorithm would underestimate the Southern Ocean chlorophyll concentrations on average by a factor of 2.5.

However, few datapoints are available at the high and low ends of the chlorophyll range. At the tail ends of the chlorophyll distribution, data from the BOPS-II and PRR instru-

Table 3. Southern Ocean Chlorophyll Algorithms Using Reflectance Ratios and Satellite-Derived Chlorophyll

Algorithm Input (X)	Formulation[a]	Coefficient a	b	c	d	e
		CZCS <1.5 mg m^{-3}				
log ($L_u(440)/L_u(555)$)	power	0.51	−1.69			
CZCS-derived chlorophyll	linear	0	2.22			
		CZCS >1.5 mg m^{-3}				
log ($L_u(520)/L_u(555)$)	power	0.78	−2.52			
log (CZCS-derived Chlorophyll)	power	0.45	0.53			
		SeaWiFS OC2V2				
log ($R_{rs}(490)/R_{rs}(555)$)	3-poly.	0.641	−2.058	−0.442	−1.140	
log (OC2V2-derived Chlorophyll)	4-poly.	0.3914	1.0176	−0.3114	0.0186	0.0610

[a]Formulations are linear, $C = a + bX$; power, $C = 10^{(a+bX)}$; three-degree polynomial (3-poly.), $C = 10^{(a+bX+cX^2+dX^3)}$; four-degree polynomial (4-poly.), $C = 10^{(a+bX+cX^2+dX^3+eX^4)}$.

ments appear to diverge. For low-chlorophyll stations (0.1 mg Chl m^{-3}) the PRR reflectance ratios tend to be lower per unit chlorophyll than the BOPS-II ratios and centered more closely around the OC2V2 algorithm. At high-chlorophyll stations (>10 mg Chl m^{-3}) the PRR reflectance ratios tend to be a bit higher than the BOPS-II ratios. Because the PRR data fit the OC2V2 wavelengths precisely (490 and 555 nm), compared to the BOPS-II (488 and 565 nm), and because instrument self-shading is a bigger problem on the BOPS-II, we have chosen to fit a polynomial line through just the PRR data. The polynomial line follows the best fit log linear regression ($r^2 = 0.83$) for most of the chlorophyll range and only curves at the tail ends of the range. This polynomial fit describes the factor of 2.5 difference but does not distort the chlorophyll retrieval from the OC2V2 algorithm at the extreme ranges where we have little data. The coefficients for the fitted lines are presented in Table 3.

The factor of 2.5 and the general consistency in the LTER data are different from recent Ross Sea results, which show that the performance of the CZCS and SeaWiFS processing algorithms depend strongly on species composition [*Arrigo et al*., 1998] (Figure 8a; lines expressed over data ranges from which algorithm were derived). Within the Antarctic Peninsula waters of the LTER we typically find large blooms of diatoms and, intermittently, cryptophytes [*Moline and Prezelin*, 1996; *Vernet et al*., 1996; *Dierssen et al*., 2000]. Even with these two different types of blooms, our data indicate that the CZCS and SeaWiFS algorithms consistently underestimate chlorophyll concentrations by roughly a factor of 2. Moreover, developing algorithms for a limited range of chlorophyll can lead to large errors in estimating biomass outside of the range.

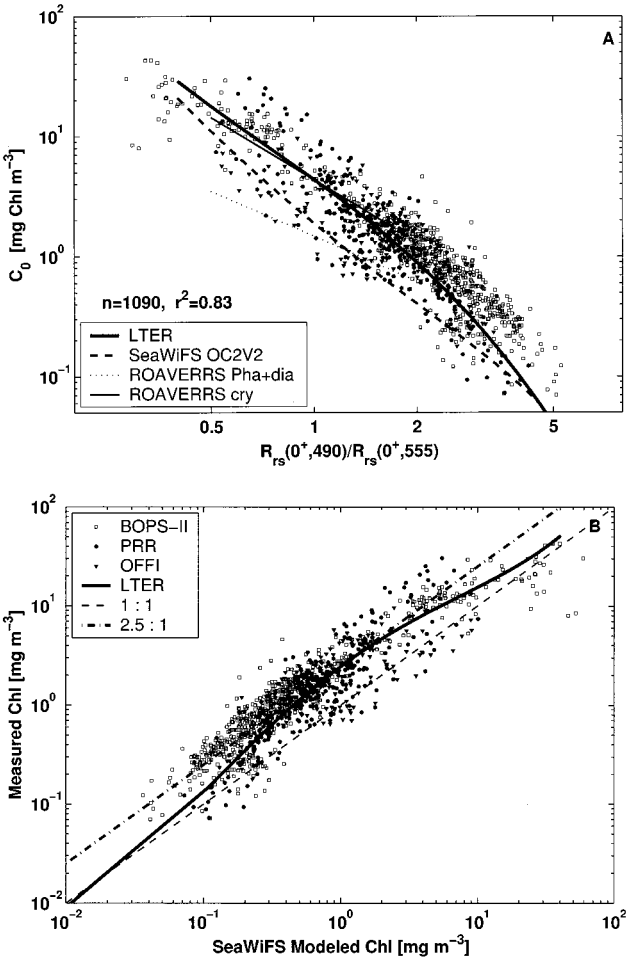

Figure 8. (a) Chlorophyll concentrations versus $R_{rs}(490)/R_{rs}(555)$ for the three LTER instruments. The thick solid line is the best fit regression line for the PRR data. Also shown are the OC2V2 algorithm used for SeaWiFS and Ross Sea ROAVERRS algorithms from *Arrigo et al*. [1998], where cryp is cryptophytes, Pha is *Phaeocystis Antarctica*, and dia is diatoms. (b) Measured chlorophyll versus chlorophyll modeled using the OC2V2 algorithm. The dashed line presents the 1:1 correlation, and the dot-dashed line presents the 2.5:1 correlation.

4. Discussion

For these waters west of the Antarctic Peninsula, blue-to-green reflectance ratios are higher than the global ratios and satellite pigment-retrieval algorithms significantly underestimate chlorophyll concentrations by at least a factor of 2. As shown in section 3, the higher Antarctic blue-to-green reflectance ratios per unit chlorophyll are due to a combination of both higher blue reflectance and lower green reflectance. Here we investigate the possible influences of the inherent optical properties (IOPs) on the differences in the LTER and Sea-

BAM reflectance spectra. Radiance reflectance is proportional to the backscattering coefficient b_b and inversely proportional to the absorption coefficient a [*Morel and Gentili*, 1991] such that

$$R_{rs} \approx \frac{f}{Q}\frac{b_b}{a}. \quad (7)$$

In order to explore the factor of 2 difference between measured and satellite-derived pigment concentrations the ratio f/Q, absorption, and backscattering are discussed below in relation to the LTER reflectance data.

4.1. Ratio f/Q

The Q factor expresses the nonisotropic character of the radiance distribution and relates a given upwelling radiance L_u to the corresponding upwelling irradiance E_u such that

$$Q = \frac{E_u}{L_u}, \quad (8)$$

where Q has been shown to be strongly dependent on the Sun angle and, to lesser degree, wavelength. The f factor, which relates $R_{rs}(0^+, \lambda)$ to the inherent optical properties of the water body, is also dependent on Sun angle. Because of the parallel dependencies of f and Q on Sun angle, the ratio of these two parameters, f/Q, has been found to be relatively stable ($\pm 20\%$) [*Gordon*, 1986; *Morel and Gentili*, 1993]. While the ratio is more constant than either of the parameters individually, f/Q ratios can still vary from 0.12 for low-pigment waters and blue wavelengths down to 0.08 for high pigment waters and red wavelengths [*Morel and Gentili*, 1993].

Modeling results suggest that there are regional differences in f/Q. In contrast to temperate regions, polar regions have large solar zenith angles (always $>40°$ at Palmer Station) and the proportion of diffuse skylight is high, especially in the blue regions of the spectrum [*Dierssen and Smith*, 1997]. *Morel and Gentili* [1993] model the changing trends in f/Q with latitude and determine that across the visible spectrum, f/Q ratios are $\sim 5\%$ greater in polar regions than in temperate regions. The latitudinal differences in f/Q ratios are more pronounced at chlorophyll >0.3 mg m^{-3}, which is generally the case for most of our LTER data (Figure 3). Because f/Q is proportional to $R_{rs}(0^+, \lambda)$ (equation (7)), a higher f/Q would result in a higher $R_{rs}(0^+, \lambda)$ for these polar waters. However, the LTER reflectance in the green is lower, not higher, than the SeaBAM data. While f/Q may play a minor role in explaining the increased reflectance in the blue, the magnitude of difference between the SeaBAM and LTER data is generally $>5\%$ (Table 2).

4.2. Absorption

The total spectral absorption coefficient a is composed of several components:

$$a = a_W + a_P + a_{DS}, \quad (9)$$

where a_W is absorption due to water, a_P is absorption due to total particulates (i.e., phytoplankton and detrital materials), and a_{DS} is absorption due to colored dissolved organic materials [*Sakshaug et al.*, 1997]. These properties are discussed below in relation to their effects on $R_{rs}(0^+, \lambda)$. Since $R_{rs}(0^+, \lambda)$ is inversely proportional to a (equation (7)), higher $a(\lambda)$ would result in lower $R_{rs}(0^+, \lambda)$.

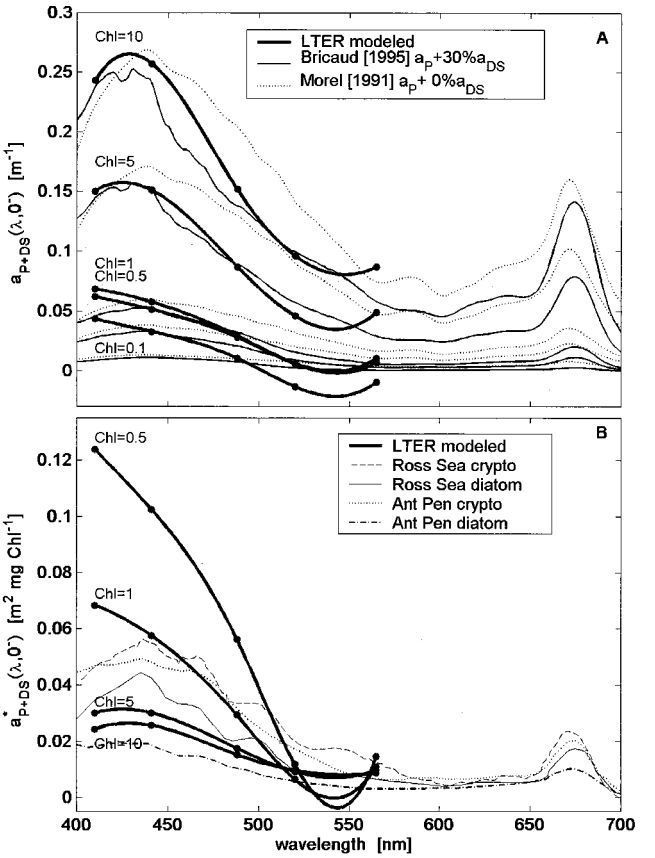

Figure 9. (a) Absorption due to particulates and dissolved organic matter $a_{P+DS}(\lambda, 0^-)$, estimated from the BOPS-II data using Gershun's law (equation (10)) and subtracting a_W [*Pope and Fry*, 1997]. Modeled estimates of $a_{P+DS}(\lambda, 0^-)$ from *Bricaud et al.* [1995] and *Morel* [1991]. Mean standard deviation is ± 0.032. (b) Pigment-specific absorption $a^*_{P+DS}(\lambda, 0^-)$ for different chlorophyll concentrations. Ross Sea data are from *Arrigo et al.* [1998], and Antarctic Peninsula data are from *Brody et al.* [1992].

To analyze the absorption characteristics of these waters, we estimated total absorption $a(0^-, \lambda)$ from the BOPS-II data using the relationship derived by *Gershun* [1936] to estimate a from the depth rate of change of the net irradiance, K_E, and the average cosine for total light, μ, where

$$a = K_E(\lambda, z)\mu(\lambda, z) \quad (10)$$

$$\mu(\lambda, z) = \frac{E_d - E_u}{E_o}. \quad (11)$$

The value of $\mu(\lambda, z)$ is estimated from the downwelling E_d, upwelling E_u, and scalar irradiances E_o (equation (11)). For the Gershun approximation, internal sources of radiant energy are assumed to be negligible.

We estimated $a(0^-, \lambda)$ from (10) using the E_d, E_u, and E_o data from the BOPS-II instrument. By subtracting a_W [*Pope and Fry*, 1997] from the total absorption we arrived at surface estimates of absorption due to particulates and colored dissolved organic materials, $a_{P+DS}(0^-, \lambda)$. As shown in Figure 9a, the magnitude of $a_{P+DS}(0^-, \lambda)$ increases with increasing chlorophyll concentration up to around 0.25 m^{-1} for chlorophyll of 10 mg Chl m^{-3}. We compared these $a_{P+DS}(0^-, \lambda)$

with modeled estimates using two different chlorophyll-specific relationships [*Morel*, 1991; *Bricaud et al*., 1995]. The shape and magnitude of the LTER $a_{P+DS}(0^-, \lambda)$ could be best approximated by using the *Bricaud et al*. [1995] model with an additional 30% $a_{DS}(0^-, \lambda)$ (modeled with an exponential decay slope of 0.02). Because the *Morel* [1991] model has higher pigment-specific absorption coefficients, this model was closest to the LTER data with no additional contribution of $a_{DS}(0^-, \lambda)$. However, both models tend to underestimate $a_{P+DS}(0^-, \lambda)$ at low pigment concentrations. We speculate that $a_{DS}(0^-, \lambda)$ is underestimated when total absorption is low and a fixed percentage (i.e., 30%) is used throughout the chlorophyll range to estimate the contribution of $a_{DS}(0^-, \lambda)$.

When the $a_{P+DS}(0^-, \lambda)$ are normalized to chlorophyll concentration (Figure 9b), the resulting pigment-specific absorption $a^*_{P+DS}(0^-, \lambda)$ tends to be high for low chlorophyll concentrations (<1 mg m^{-3}) and low for high chlorophyll concentrations (5–20 mg m^{-3}). This is consistent with pigment package effects in which pigment-specific absorption decreases with increasing chlorophyll concentrations. We have also compared our estimates of $a^*_{P+DS}(0^-, \lambda)$ with previously published absorption measurements in the Southern Ocean. In the LTER region, diatoms are the major bloom-forming plankton, although cryptophytes are occasionally dominant in the water column [*Kozlowski et al*., 1995; *Moline and Prezelin*, 1996; *Dierssen et al*., 2000]. For cryptophytes collected both in the Antarctic Peninsula and the Ross Sea (Figure 9b) [*Brody et al*., 1992; *Arrigo et al*., 1998], $a^*_P(0^-, \lambda)$ was quite high and in the range measured for temperate species.

Diatoms from these two regions, however, had vastly different $a^*_P(0^-, \lambda)$. In the Ross Sea the diatom $a^*_P(0^-, \lambda)$ spectra was found to be quite similar to cryptophytes; whereas in the Antarctic Peninsula, $a^*_P(0^-, \lambda)$ was low for the diatom populations [*Mitchell and Holm-Hansen*, 1991; *Brody et al*., 1992]. The discrepancy in absorption between the two diatom populations can be explained by comparing the various cell sizes of the organisms. The diatoms reported for Antarctic Peninsula waters tend to be much larger (diameter >20 μm) [*Brody et al*., 1992] than the diatoms reported for Ross Sea waters (total volume of 30 μm^3) [*Arrigo et al*., 1998]. For the LTER data we find that as chlorophyll increases, the cell sizes also increase. For chlorophyll >5 mg m^{-3}, over 90% of the chlorophyll occurs in cells >20 μm. Our low estimates of $a^*_{P+DS}(0^-, \lambda)$ at high chlorophyll concentrations are therefore consistent with large diatoms generally associated with Antarctic Peninsula waters.

Because absorption is inversely proportional to reflectance (equation (7)), lower absorption results in greater reflectance. Consistent with past findings in the western Antarctic Peninsula region [*Mitchell and Holm-Hansen*, 1991], we postulate that low $a^*_{P+DS}(0^-, \lambda)$, especially at high chlorophyll concentrations, could result in the increased $R_{rs}(0^+, \lambda)$ observed in the blue region of the spectrum. However, absorption generally influences the blue and red portions of the spectrum and not the green, where we observe a low reduced reflectance at 555 nm. If the phytoplankton contained pigments that absorbed highly in the green region of the spectra, higher $a_p(0^-, 555)$ could hypothetically result in a lower $R_{rs}(0^+, 555)$. Of the major bloom-forming plankton in this region, diatoms and cryptophytes both contain pigments that can absorb light in the green region of the spectra (500–600 nm). However, neither the LTER data nor the other Southern Ocean data give any indication of anomalously high absorption in the green region of the spectrum, which would cause the depressed $R_{rs}(0^+, 555)$. This suggests that high $a_p(555)$ is unlikely to be the cause of the low measurements of $R_{rs}(0^+, 555)$ with increasing chlorophyll concentrations. Therefore we hypothesize that backscattering must also play an important role in the factor of 2 of difference in remote sensing pigment retrieval algorithms for this region.

4.3. Backscattering

With increased concentration of total particulates in a water body the amount of backscattered light generally increases at all wavelengths. However, when the particles are predominantly algae, certain parts of the visible spectra (i.e., blue and red) are highly absorbed and the resulting shape of the $R_{rs}(0^+, \lambda)$ curve is low in blue and red and high in green (as shown in the high-chlorophyll SeaBAM data, Figure 4a). The presence of the so-called $R_{rs}(0^+, \lambda)$ spectral hinge point in which high- and low-chlorophyll $R_{rs}(0^+, \lambda)$ cross at ~500 nm has been a commonly observed characteristic of ocean color data sets. However, the LTER green reflectance is significantly lower than SeaBAM, especially as chlorophyll concentrations increase above 5 mg Chl m^{-3}. Because backscattering is proportional to reflectance (equation (7)), reduced backscattering could explain the low green reflectance observed in the LTER data.

Because of the low refractive index of living cells relative to water [*Kirk*, 1994], backscattering from phytoplankton is considered to be minimal. Theoretical studies suggest that most of particulate backscattering is due to detrital particles <0.6 μm (i.e., Koike particles) and not to phytoplankton [*Morel and Ahn*, 1990; *Stramski and Kiefer*, 1991; *Ulloa et al*., 1994; *Balch et al*., 1998]. Nevertheless, phytoplankton concentrations have been found to covary with the amount of backscattered light. *Ulloa et al*. [1994] present an explanation for this paradox by showing that an inverse relationship exists between pigments and the shape of the total particle size distribution, which is, in turn, the principle control on the ratio of backscattering to total scattering. If concentrations of minute backscattering detrital particles covary with phytoplankton, backscattering will increase with higher phytoplankton concentrations. Because of their minute size, submicron detritus have only recently been demonstrated to occur in large numbers in most regions of the world's ocean [*Koike et al*., 1990] and little is known of their abundance in the Antarctic.

If backscattering is found to be lower in the Southern Ocean, then one could hypothesize that concentrations of submicron detrital particles are also low. The relationships between other submicron populations (e.g., viral and microbial) and phytoplankton in the Antarctic may be fundamentally different from other marine habitats. *Karl et al*. [1996] have shown that Antarctic bacterial productivity is generally uncoupled to phytoplankton concentrations and is consistently low relative to phytoplankton productivity. Even during the spring bloom, bacterial biomass are <1–2% of the contemporaneous phytoplankton standing stock compared to ≥ 10% for most other oceanic regions [*Karl et al*., 1996]. Moreover, virus particle abundance has also been found to be consistently low in the surface waters of the Antarctic [*Karl et al*., 1996]. This is not unique to Antarctic Peninsula waters but is ubiquitous for all Southern Ocean ecosystems studied [*Lancelot et al*., 1989; *Cota et al*., 1990; *Zdanowski and Donachie*, 1993]. Given that microbial activities may contribute to the formation of submicron detritus with a low refractive index (i.e., Koike particles) [*Stramski and Kiefer*, 1991], the reduced microbial populations

in the Antarctic may be correlated with a low abundance of submicron detritus that causes most of the backscattering in the ocean. Therefore we postulate that low backscattering at high chlorophyll may be a feature of parts of the Southern Ocean and may influence the performance of ocean color algorithms. Future efforts will be directed at characterizing the absorption and backscattering coefficients in relation to the reflectance spectra and the factor of 2 difference in pigment retrieval algorithms.

Note added in proof. While this paper was in press, a new algorithm was developed for retrieving chlorophyll from SeaWiFS data. The Ocean Color 4 wavelength version 4 (OC4V4) algorithm uses the maximum band ratio of R_{rs} (443>490>510) over R_{rs} (555). For these LTER data, chlorophyll estimated with the OC4V4 algorithm varies by only a few percent from that estimated with the OC2V2 algorithm for most of the LTER data. The algorithms only differ significantly at the tail ends of the distribution (>10 mg Chl m^{-3} and <0.1 mg Chl m^{-3}). The algorithm in Table 3 for estimating Southern Ocean chlorophyll from OC2V2-derived chlorophyll does not need to be modified to be applicable to OC4V4-derived chlorophyll. All other conclusions presented in this paper are unaffected by the new algorithm and remain valid.

Acknowledgments. This research was supported by NASA training grants NGT-30063 (Earth System Science Fellowship) and NGT-40005 (California Space Institute) to H. Dierssen and NSF grant OPP90-11927 and NASA grant NAGW 290-3 to R. C. Smith. Karen Baker provided data management, and Sharon Stammerjohn, Maria Vernet, and Brad Seibel gave helpful comments on the manuscript. Dave Menzies carried out instrument repair and optical calibration. Also acknowledged are the many people who helped acquire the data at sea, in particular, Tim Newberger, Phil Handley, and Janice Jones. We further wish to thank the anonymous reviewers for their helpful comments on this manuscript.

References

Aas, E., and B. Korsbo, Self-shading effect by radiance meters on upward radiance observed in coastal waters, *Limnol. Oceanogr.*, *42*, 968–974, 1997.

Arrigo, K. R., D. H. Robinson, D. L. Worthen, B. Schieber, and M. P. Lizotte, Bio-optical properties of the southwestern Ross Sea, *J. Geophys. Res.*, *103*, 21,683–21,695, 1998.

Austin, R. W., and G. Halikas, The index of refraction of seawater, 121 pp., Scripps Inst. of Oceanogr., La Jolla, Calif., 1976.

Balch, W., et al., Light scattering by viral suspensions, in *Proceedings Ocean Optics XIV* [CD-ROM], edited by S. Ackleson, and J. Campbell, Off. of Nav. Res., Kailua-Kona, Hawaii, 1998.

Bricaud, A., M. Babin, A. Morel, and H. Claustre, Variability in the chlorophyll-specific absorption coefficients of natural phytoplankton: Analysis and parameterization, *J. Geophys. Res.*, *100*, 13,321–13,332, 1995.

Brody, E., B. G. Mitchell, O. Holm-Hansen, and M. Vernet, Species-dependent variations of the absorption coefficient in the Gerlache Strait, *Antarct. J. U.S.*, *27*, 160–162, 1992.

Cota, G. F., S. T. Kottmeier, D. H. Robinson, W. O. Smith, and C. W. Sullivan, Bacterioplankton in the marginal ice zone of the Weddell Sea: Biomass, production, and metabolic activities during austral autumn, *Deep Sea Res., Part A*, *37*, 1145–1167, 1990.

Dierssen, H. M., and R. C. Smith, Estimation of irradiance just below the air-water interface, in *Proceedings Ocean Optics XIII*, edited by S. Ackleson and R. Frovin, *Proc. SPIE Int. Soc. Opt. Eng.*, *2963*, 204–209, 1997.

Dierssen, H. M., and R. C. Smith, Case 2 Antarctic coastal waters: The bio-optical properties of surface meltwater, in *Proceedings Ocean Optics XV* [CD-ROM], edited by S. Ackleson and J. Marra, Off. of Nav. Res., Kailua-Kona, Hawaii, 2000.

Dierssen, H. M., R. C. Smith, and M. Vernet, Optimizing models for remotely estimating primary production in Antarctic coastal waters, *Antarct. Sci.*, *12*, 20–32, 2000.

Fenton, N., J. Priddle, and P. Tett, Regional variations in bio-optical properties of the surface waters in the Southern Ocean, *Antarct. Sci.*, *6*, 443–448, 1994.

Gershun, A. A., Fundamental ideas of the theory of a light field (vector methods of photometric calculations) (in Russian), *Izv. Akad. Nauk SSSR, Ser. Fiz.*, *1*, 417–430, 1936.

Gordon, H. R., Ocean color remote sensing: Influence of the particle scattering phase function and the solar zenith angle (abstract), *Eos Trans. AGU*, *67*(44), 1055, 1986.

Gordon, H. R., and K. Ding, Self shading of in-water optical instruments, *Limnol. Oceanogr.*, *37*, 491–500, 1992.

Gordon, H. R., and A. Y. Morel, *Remote Assessment of Ocean Color for Interpretation of Satellite Visible Imagery: A Review*, Springer-Verlag, New York, 1983.

Karl, D. M., J. R. Christian, and J. E. Dore, Microbiological oceanography in the region west of the Antarctic Peninsula: Microbial dynamics, nitrogen cycle and carbon flux, in *Foundations for Ecosystem Research West of the Antarctic Peninsula*, *Antarct. Res. Ser.*, vol. 70, edited by R. M. Ross, E. E. Hofmann, and L. B. Quetin, pp. 303–332, AGU, Washington, D. C., 1996.

Kirk, J. T. O., *Light and Photosynthesis in Aquatic Ecosystems*, Cambridge Univ. Press, New York, 1994.

Koike, I., S. Hara, T. Terauchi, and K. Kogure, Role of submicrometer particles in the ocean, *Nature*, *345*, 242–244, 1990.

Kozlowski, W., S. K. Lamerdin, and M. Vernet, Palmer LTER: Predominance of cryptomonads and diatoms in Antarctic coastal waters, *Antarct. J. U.S.*, *30*, 267–268, 1995.

Lancelot, C., G. Billon, and S. Mathot, *Ecophysiology of Phyto- and Bacterioplankton Growth in the Southern Ocean*: *Belgian Scientific Research Programme on Antarctica Scientific Results of Phase One* (*Oct 85–Jan 89*), 97 pp., Belgium Sci. Res. Programme on Antarct., Brussels, 1989.

Laws, E. A., and J. W. Archie, Appropriate use of regression analysis in marine biology, *Mar. Biol.*, *65*, 13–16, 1981.

Mitchell, B. G., Predictive bio-optical relationships for polar oceans and marginal ice zones, *J. Mar. Syst.*, *3*, 91–105, 1992.

Mitchell, B. G., and O. Holm-Hansen, Bio-optical properties of Antarctic Peninsula waters: Differentiation from temperate ocean models, *Deep Sea Res., Part A*, *38*, 1009–1028, 1991.

Mobley, C. D., *Light and Water: Radiative Transfer in Natural Waters*, Academic, San Diego, Calif., 1994.

Moline, M., and B. B. Prezelin, Long-term monitoring and analyses of physical factors regulating variability in coastal Antarctic phytoplankton biomass, in situ productivity and taxonomic composition over subseasonal, seasonal, and interannual time scales, *Mar. Ecol. Prog. Ser.*, *145*, 143–160, 1996.

Morel, A., Light and marine photosynthesis: A spectral model with geochemical and climatological implications, *Prog. Oceanogr.*, *26*, 263–306, 1991.

Morel, A., and Y. H. Ahn, Optical efficiency factors of free-living marine bacteria: Influence of bacterioplankton upon the optical properties and particulate organic carbon in oceanic waters, *J. Mar. Res.*, *48*, 145–175, 1990.

Morel, A., and B. Gentili, Diffuse reflectance of oceanic waters: Its dependence on Sun angle as influenced by the molecular scattering contribution, *Appl. Opt.*, *30*, 4427–4438, 1991.

Morel, A., and B. Gentili, Diffuse reflectance of oceanic waters, II, Bidirectional aspects, *Appl. Opt.*, *32*, 6864–6879, 1993.

Mueller, J. L., Comparison of irradiance immersion coefficients for several marine environmental radiometers (MERs), in *Case Studies for SeaWiFS Calibration and Validation*, *Part 3*, vol. 27, edited by S. B. Hooker, E. R. Firestone, and J. G. Acker, *NASA Tech. Memo.*, *104566*, 46 pp., 1995.

Mueller, J. L., and R. W. Austin, *Ocean Optics Protocols for SeaWiFS Validation*, *Revision 1*, vol. 25, *NASA Tech. Memo.*, *104566*, 67 pp., 1995.

O'Reilly, J. E., et al., Ocean color chlorophyll algorithms for SeaWiFS, *J. Geophys. Res.*, *103*, 24,937–24,953, 1998.

Pope, R., and E. Fry, Absorption spectrum of pure water, 2, Integrating cavity measurements, *Appl. Opt.*, *36*, 8710–8723, 1997.

Sakshaug, E., et al., Parameters of photosynthesis: Definitions, theory and interpretation of results, *J. Plankton Res.*, *19*, 1637–1670, 1997.

Smith, R. C., and K. S. Baker, The analysis of ocean optical data, *Proc. SPIE Int. Soc. Opt. Eng.*, *489*, 119–126, 1984.

Smith, R. C., and K. S. Baker, Analysis of ocean optical data II, *Proc. SPIE Int. Soc. Opt. Eng*., *637*, 95–107, 1986.

Smith, R. C., K. S. Baker, and P. Dustan, Fluorometer techniques for measurement of oceanic chlorophyll in the support of remote sensing, Visibility Lab., Scripps Inst. of Oceanogr., San Diego, Calif., 1981.

Smith, R. C., D. W. Menzies, and C. R. Booth, Oceanographic Bio-optical Profiling System II, *Proc. SPIE Int. Soc. Opt. Eng*., *2963*, 777–786, 1997.

Stramski, D., and D. A. Kiefer, Light scattering by microorganisms in the open ocean, *Prog. Oceanogr*., *28*, 343–393, 1991.

Stramski, D., R. Reynolds, and B. G. Mitchell, Relationships between the backscattering coefficient, beam attenuation coefficient and particulate organic matter concentrations in the Ross Sea, in *Proceedings Ocean Optics XIV* [CD-ROM], edited by S. Ackleson and J. Campbell, Off. of Nav. Res., Kailua-Kona, Hawaii, 1998.

Sullivan, C. W., K. R. Arrigo, C. R. McClain, J. C. Comiso, and J. Firestone, Distributions of phytoplankton blooms in the Southern Ocean, *Science*, *262*, 1832–1837, 1993.

Ulloa, O., S. Sathyendranath, and T. Platt, Effect of the particle-size distribution on the backscattering ratio in seawater, *Appl. Opt*., *33*, 7070–7077, 1994.

Vernet, M., W. Kozlowski, and T. Ruel, Palmer LTER: Temporal variability in primary productivity in Arthur Harbor during the 1994/1995 growth season, *Antarct. J. U.S*., *30*, 266–267, 1996.

Waters, K. J., and R. C. Smith, Palmer LTER: A sampling grid for the Palmer LTER program, *Antarct. J. U.S*., *27*, 236–239, 1992.

Waters, K. J., R. C. Smith, and M. R. Lewis, Avoiding ship-induced light-field perturbation in the determination of oceanic optical properties, *Oceanography*, *November*, 18–21, 1990.

Zdanowski, M. K., and S. P. Donachie, Bacteria in the sea-ice zone between Elephant Island and the South Orkneys during the Polish sea-ice expedition, *Polar Biol*., *13*, 245–254, 1993.

Zibordi, G., and G. Z. Ferraro, Instrument self-shading in underwater optical measurements: Experimental data, *Appl. Opt*., *34*, 2750–2754, 1995.

H. M. Dierssen and R. C. Smith, Institute for Computational Earth System Science, Department of Geography, University of California, Santa Barbara, CA 93106. (dierssen@icess.ucsb.edu)

(Received January 6, 1999; revised January 26, 2000; accepted April 18, 2000.)